ACS APPLIED MATERIALS & INTERFACES

Research Article

www.acsami.org

Polypyrrole-Coated Chainlike Gold Nanoparticle Architectures with the 808 nm Photothermal Transduction Efficiency up to 70%

Min Lin,[†] Changrun Guo,[‡] Jing Li,[†] Ding Zhou,[†] Kun Liu,[†] Xue Zhang,[†] Tianshu Xu,[‡] Hao Zhang,*[,†] Liping Wang,*[,‡] and Bai Yang[†]

[†]State Key Laboratory of Supramolecular Structure and Materials, College of Chemistry, Jilin University, Changchun 130012, People's Republic of China

[‡]College of Life Science, Jilin University, Changchun 130012, People's Republic of China

Supporting Information

ABSTRACT: Aqueous Au nanoparticles (NPs) are employed as the building blocks to construct chainlike self-assembly architectures, which greatly enhance the photothermal performance at 808 nm. Biocompatible polypyrrole (PPy) is further adopted as the package material to coat Au NP chains, producing stable photothermal agents. As a result of contributions from chainlike Au, the PPy shell, as well as the Au−PPy composite structures, the capability of photothermal transduction at 808 nm is greatly enhanced, represented by the high photothermal transduction efficiency up to 70%. Primary animal experiment proves that the current composite photothermal agents are efficient in inhibiting tumor growth under an 808 nm irradiation, showing the potentials for in vivo photothermal therapy.

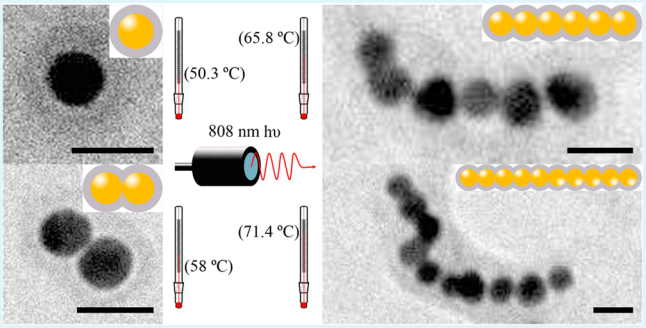

KEYWORDS: *nanoparticle, photothermal effect, self-assembly, polypyrrole, nanocomposite*

INTRODUCTION

Photothermal therapy on the basis of the conversion of near-infrared (NIR) irradiation into heat energy by nanomaterials has attracted much attention in the past few years because it permits disease treatment via noninvasive and targeted approaches.[1−3] This capability shows the potentials in establishing novel diagnostic and therapeutic methodologies, such as optically induced drug release and selective treatment of tumors, by minimizing the damage to healthy tissues and organs.[4−11] The tested photothermal nanomaterials include organic compounds,[12] polymers,[13−15] carbon materials,[16−18] inorganic materials,[19−22] and their composites.[23] Among these, the inorganic nanomaterials, mainly composed of noble metals and copper chalcogenides, are ones of most studied photothermal agents, owing to their high photothermal transduction efficiency (η).[24−26] In addition, gold (Au)-based nanomaterials are the focus of current research because of their flexibility in morphology control.[27−29] Au nanorods,[30,31] nanoshells,[32] nanostars,[33,34,48−52] and nanocages[28,35] strongly absorb NIR light and have been proved to be good photothermal agents, but the limitations in repeatable preparation and poor structure stability upon NIR irradiation shed the doubt on further applicability.[36,37] In comparison, spherical Au nanoparticles (NPs) possess good structure stability and can be prepared in large scale with good repeatability, despite the low extinction at the NIR region. For example, Au NPs have an extinction coefficient approximating to 0 at 808 nm. Nevertheless, Au NPs are potential candidates as photothermal agents, if the extinction is tunable to NIR.

Multiplex assembly is the current workhorse in integrating and enhancing the functionalities of given materials.[38,39] For example, self-assembly and co-assembly of NPs lead to diversified architectures and the subsequent functional improvement.[40] Meanwhile, polymer coating of instable NPs and their self-assembly architectures further enhance the structural stability.[36,37,41] To improve the photothermal transduction effect of Au NPs in the NIR region, it is reasonable to modulate the plasmon resonance absorption of Au via a self-assembly strategy. We have demonstrated a controlled growth of chains composed of aqueous Au NPs by virtue of interparticle electrostatic repulsion, which led to a significant shift of the extinction to the NIR region.[42] However, the colloidal stability of the chainlike Au NP architectures is poor. Serious aggregation occurs in storing the Au chains, which limits both the academic studies and the practical applications as photothermal agents. Herein, biocompatible polypyrrole (PPy) is adopted as the agent to coat Au NP chains, producing stable photothermal self-assembly architectures. As a result of contributions from the chainlike Au structure, PPy shell, as well as the Au−PPy composite structures, the capability of

Received: February 2, 2014
Accepted: March 24, 2014
Published: March 24, 2014

   dx.doi.org/10.1021/am500715f | ACS Appl. Mater. Interfaces 2014, 6, 5860−5868

photothermal transduction at 808 nm is greatly enhanced, represented by the η up to 70%. Primary animal experiment proves that the PPy-coated Au chains are effective in inhibiting tumor growth under an 808 nm irradiation, acting as the promising candidates for in vivo photothermal therapy.

EXPERIMENTAL SECTION

Materials. 1-Aminopyrrole (Py, 98%, Alfa Aesar), hydrogen tetrachloroaurate(III) ($HAuCl_4$, 99.9%, Alfa Aesar), sodium citrate (99.0%, Sigma), dodecyl sodium sulfate (SDS, 99%, Alfa Aesar), $(NH_4)_2S_2O_8$ (98%, Alfa Aesar), hexadecyltrimethylammonium chloride (CTAC, 25% in water, Fluka), styrene (St, 99%, Sigma), divinylbenzene (DVB, 80%, Fluka), 2,2′-azobis(2-methylpropionamidine) dihydrochloride (AAPH, 97%, Aladdin), acrylic acid (AA, 99%, TCI), *N*-isopropylacrylamide (NIPAM, 99%, J&K CHEMICAL), and *N*,*N*-methylenebisacrylamide (MBA, 99%, Sigma) were used as received. In all experiments, deionized water was used.

Citrate-Stabilized Au NPs. The spherical Au NPs were prepared in boiling water using citrate as the reducing agent cum capping ligand according to the previous method.[47] A 0.3 mL portion of 0.1 M $HAuCl_4$ was added into 170 mL of water. After addition of 5 mL of 2% sodium citrate solution, the solution was heated to boiling and maintained for 10 min. The mass concentration of the Au solution was 33.8 μg/mL.

PPy-Coated Au NP Chains. A 3 mL 100 mM Py aqueous solution was added into 100 mL of Au NP solution under vigorous stirring for 5 min to induce the growth of NP chains at room temperature. The increase of chain length was monitored by the UV−vis absorption spectra. After the NP chains grow to a specific length, 6 mL of 40 mM SDS, 6 mL of 100 mM Py, and 10 mL of 6 mM acidic $(NH_4)_2S_2O_8$ were added in turn to prevent the further growth of chains but initiate polymerization. The reaction mixture was incubated at room temperature for 24 h to complete the polymerization. The products were centrifuged at 15 000 rpm for 20 min to discard the supernatant, which excluded the influence of PPy NP self-nucleation on the photothermal effect. The collected Au chains were redispersed in 10 mL of deionized water, which was stable in water for months without obvious precipitation.

Decorating the Composite Au NP Chains with Other Polymers. The secondary coating of PS-*co*-PDVB was performed as follows: 60 μL of 3 M CTAC was added into 10 mL of as-prepared composite Au chains under mechanical stirring. The temperature of the solution was raised to 35 °C, and 20 μL of St and 10 μL of DVB were added under stirring. After the temperature was raised to 70 °C, 40 μL of 0.1 M aqueous AAPH was added to initiate the polymerization. The polymerization proceeded for 2 h. The products were centrifuged at 15 000 rpm for 20 min to discard the supernatant. The precipitates were dispersed in 15 mL of deionized water.

To further coat the composite Au chains with PNIPAM, the solution of PS-*co*-PDVB/PPy-coated Au chains was purged with nitrogen for 15 min, followed by addition of 0.1698 g of NIPAM and 0.022 g of MBA. After another 15 min purging, the nitrogen flow was removed and 300 μL of 0.1 M AAPH was added to initiate polymerization. 7−10 min later, the clear solution became turbid and the polymerization was allowed to proceed for 3 h at 70 °C. Finally, the mixture was cooled down to room temperature under stirring. To remove unreacted monomers, oligomers, and Au-free microgels, the mixture was diluted with 15 mL of water and centrifuged at 4000 rpm for three times. The precipitates were collected and dispersed in water. Using 0.02 mL of AA rather than 0.1698 g of NIPAM, PAA was decorated on the composite Au chains, which achieved a carboxyl surface for further bioconjugation.

Cytotoxicity Assay and Photothermal Effect of PPy-Coated Au Chains. The hepatic stellate cells (HSC-T6) and hepatoma cells (HEPG2) were cultured in standard cell media. Cells were incubated with different concentrations of PPy-coated Au chains for 24 h. The cell viability was evaluated for HSC-T6 and HEPG2 by a standard methyl thiazolyl tetrozolium (MTT) assay on 96-well plates; 570 nm was the exact wavelength for MTT assay. To exclude the background absorbance of Au NPs, a control group without cells was measured by fixing other experimental parameters. In the MTT assay, this background was deducted. In studying the photothermal effect, HEPG2 cells were incubated with and without 0.25 mg/mL PPy-coated Au chains for 4 h, and exposed to an 808 nm NIR laser with different power densities for 3 min. The plates were analyzed for cell viability using MTT assay. Each experiment was repeated three times.

Animal Experiments. Male Kunming mice were injected with 0.2 mL of a 1×10^7 H22 cell suspension in 0.9 % saline on the left shoulders. For the photothermal therapy, mice bearing H22 tumors were injected with 0.1 mL of 0.5 mg/mL PPy-coated Au chains. The control groups were injected with the same volume of saline. Mice with and without PPy-coated Au chains were irradiated by an 808 nm NIR laser with the power density of 2 W/cm^2 for 3 min. Fourteen days later, some of the mice were killed and the tumors were taken out for weighing and photographing. We chose hepatic carcinoma because H22 cells could be cultured in large quantity (10^7) and the tumor model could be established with unimmunocompromised Kunming mice. If HEPG2 was used for plantation, nude mice should be adopted in order to establish the tumor model, which was limited by the experimental conditions. Consequently, mice bearing H22 were adopted for the primary animal experiments to show the capability of our photothermal agents for inhibiting tumor growth.

Characterization. UV−visible absorption spectra were obtained using a UV-3600 UV−vis spectrophotometer at room temperature under ambient conditions. Transmission electron microscopy (TEM) was conducted using a Hitachi H-800 electron microscope at an acceleration voltage of 200 kV with a CCD camera. Dynamic light scattering (DLS) measurements were performed using a Zetasizer NanoZS (Malvern Instruments). In the study of photothermal effect, an 808 nm diode laser (LEO photonics Co. Ltd) was employed with the output power tunable from 0 to 10 W/cm^2. The temperature increment under laser irradiation is determined in a quartz cell with tin foil capped to prevent the vaporization of water (Figure S1, Supporting Information). A 2.0 mL portion of solution was added into a $1 \times 1 \times 4$ cm quartz pool and irradiated by an 808 nm laser with the output power of 3.5 W/cm^2 for 5 min. The variation of the temperature was immediately measured after irradiation. The concentration effect was studied by diluting the PPy-coated Au NP chains to specific concentrations. The output power and irradiation duration were fixed at 3.5 W/cm^2 and 5 min, respectively. The effect of output power was revealed by irradiating the PPy-coated Au NP chains with a specific output power for 2 min. The concentration of Au was 33.8 μg/mL. As a comparison, the composite Au chains were also irradiated using a 660 nm laser with the output power of 2 W/cm^2 (Table S3, Supporting Information).

RESULTS AND DISCUSSION

In our experiment, the growth of Au NP chains is induced through the addition of pyrrole (Py) into the aqueous solution of citrate-stabilized Au NPs (see the Experimental Section). The average diameter of the Au NPs is 14 nm. The length of NP chains is controllable by altering the Py content and the duration of chain growth (Figures S2 and S3, Supporting Information). With increasing the length of NP chains, an obvious shift of Au extinction toward the NIR region is found. As demonstrated in our previous work,[42] aqueous Au NPs are able to self-assemble into chainlike architectures in the presence of electrolytes and/or water-miscible solvents. As an electrolyte, Py is capable of inducing NP self-assembly, which adsorbs on the NPs and greatly lowers the interparticle electrostatic repulsion. Because the decrease of long-range electrostatic repulsion is more obvious than short-range dipolar attraction, an anisotropic chain growth is triggered.[42] Although electrostatic repulsion is isotropic, it can greatly enforce the anisotropic self-assembly in the presence of anisotropic dipolar interaction. When the NP chains grow to a specific length, a

protective PPy shell polymerizes around each NP chain. After 24 h of incubation at room temperature to complete the polymerization, PPy-coated chainlike Au NP architectures are prepared (Figure 1). The chain length distribution profile

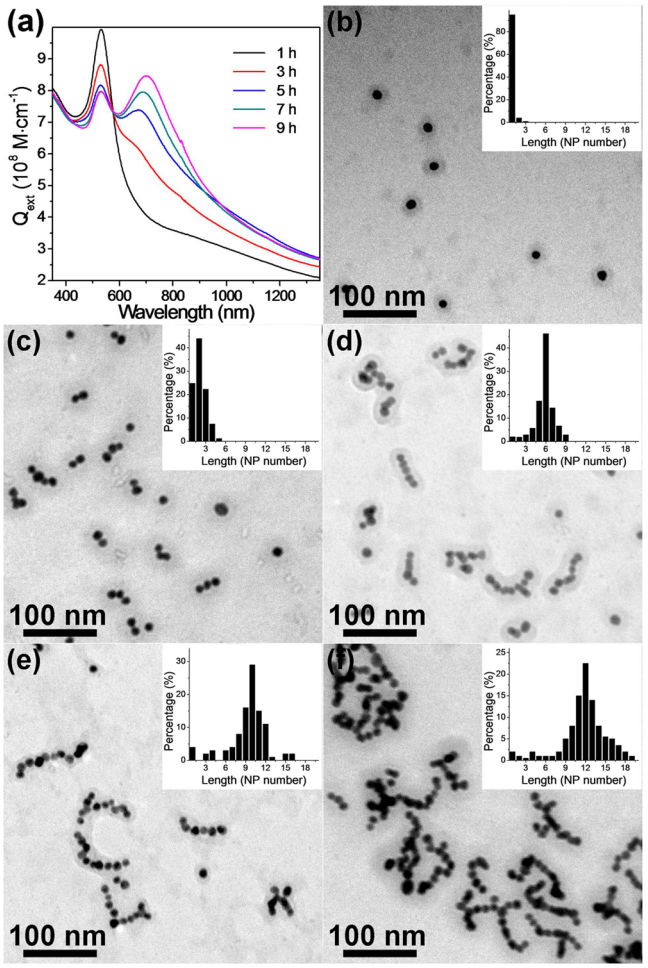

Figure 1. Extinction spectra (a) and TEM images (b–f) of the PPy-coated Au NP chains with different lengths that are prepared by adding 150 μL of Py into 5 mL of Au solution, aging for 1 (b), 3 (c), 5 (d), 7 (e), and 9 (f) h, and adding $(NH_4)_2S_2O_8$ to initiate polymerization. The Au NP concentration is 33.8 μg/mL. The average length is 1, 3, 6, 10, and 12 NPs, respectively. Insets: the distribution profile of the Au chains. 200 chains are counted.

reveals that the number of NPs in the composite Au chains is controllable (Figure 1, insets). The thickness of the PPy shell is also adjustable by altering the concentration of Py (Figure 2). The PPy coating greatly improves the structural stability of Au chains. No obvious aggregation and spectral shift are found even after months of storage in water (Figure S4, Supporting Information).

The PPy-coated chainlike Au NP architectures exhibit good photothermal effect. When irradiated by an 808 nm laser, a dramatic temperature increment of the solution is observed (Figure 3). Temperature increment elevates as the composite architecture concentration and laser power increase (Figure 3a–c). In addition, a 660 nm laser is also capable of elevating the solution temperature (Figure 3b), because the composite architectures possess improved extinction in the NIR region between 650 and 900 nm. To reduce the tissue self-absorption and the damage to the organism, an 808 nm laser is employed

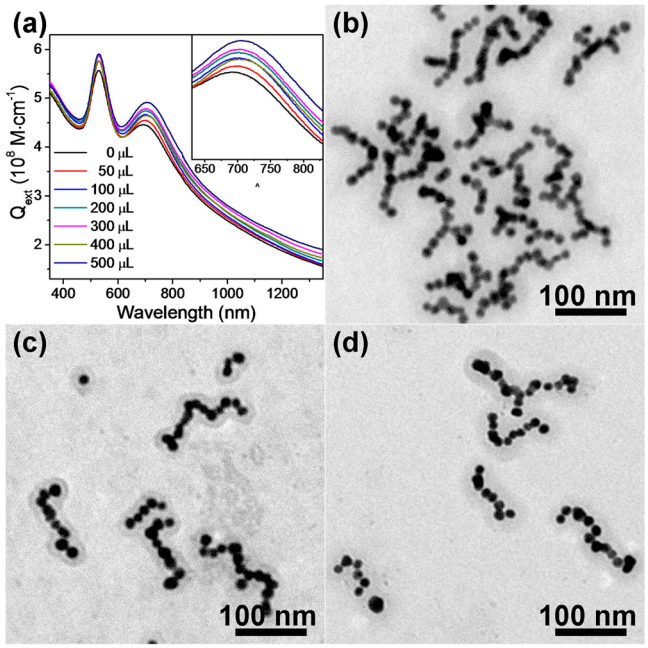

Figure 2. Extinction spectra (a) and TEM images (b–d) of the Au NP chains with different thicknesses of PPy shell. To induce the self-assembly of Au NPs, 150 μL of Py is added into 5 mL of Au solution and aged for 8 h. 100 (b), 300 (c), and 500 (d) μL of Py and 0.68 mg of $(NH_4)_2S_2O_8$ are further added to produce the PPy shell with the thickness of 7.8, 12.4, and 19.7 nm, respectively.

in the following investigation. Figure 3d compares the temperature increment of the composite Au chains with different lengths by fixing the amount of Au and PPy. After 5 min of irradiation with a 3.5 W/cm^2 laser, the solution of single NP-based composites exhibits a temperature increment of 26.4 °C, whereas the composites with an average chain length of 2, 4, 6, 10, and 12 NPs elevate the temperature 28.4, 29.2, 30.3, 32.8, and 34.4 °C, respectively. This result clearly indicates that the composite architectures with longer NP chains possess better photothermal performance. The photothermal stability of composite architectures is indicated in Figure 4a,b. After six cycles of heating and cooling under 3.5 W/cm^2 laser irradiation, only a slight decrease in the absorption spectrum and the final temperature elevation are observed, showing the good photothermal stability of PPy-coated chainlike architectures.

On the basis of time-dependent temperature increment and energy exchange equilibrium, the η of bare and PPy-coated Au chains with different lengths is calculated according to eq 1 (Figure 5, S5 (Supporting Information), and Table 1)[43]

$$\eta = \frac{hS(T_{max} - T_{surr}) - Q_0}{P(1 - 10^{-A_{808}})} \quad (1)$$

where h is heat transfer coefficient, S is the surface area of the container, T_{max} is the equilibrium temperature, T_{surr} is the ambient temperature, Q_0 represents the heat generated by NPs and quartz cell under laser irradiation, P is incident laser power, and A_{808} is the absorption intensity of NPs at 808 nm. In the absence of a PPy shell, the η increases from 17.8% to more than 70% after assembling the isolated NPs into chains (Table 1). The improved photothermal performance results from the plasmon coupling of the neighboring NPs within the Au chains, which leads to the shift of the Au extinction toward NIR. As a result, the η is greatly improved for the NP chains with

dx.doi.org/10.1021/am500715f | ACS Appl. Mater. Interfaces 2014, 6, 5860–5868

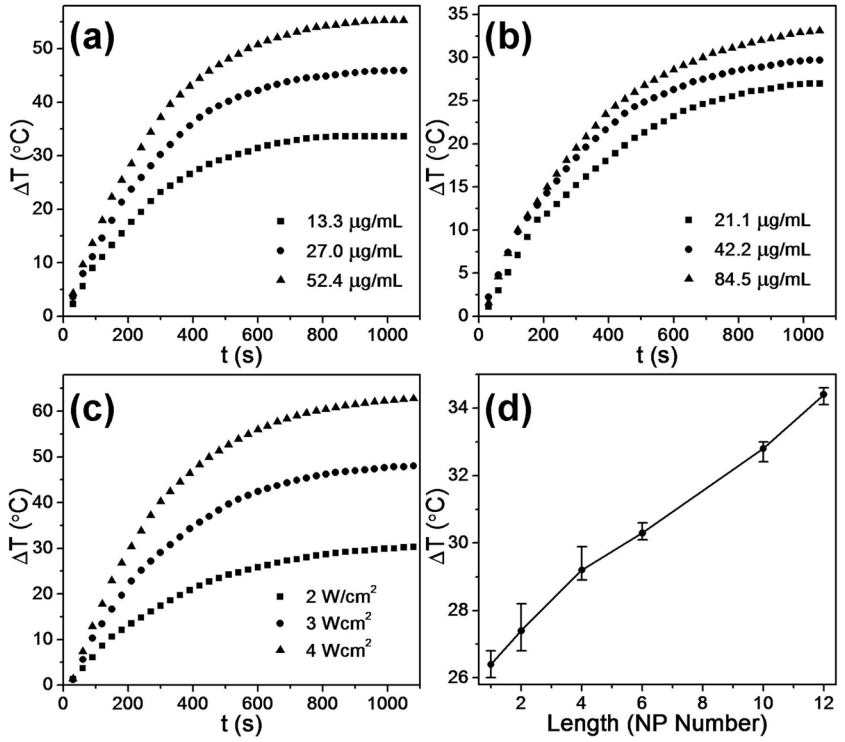

Figure 3. (a–c) The temperature increment versus irradiation time of the Au chains composed of 10 NPs. (a) Different concentrations under a 3.5 W/cm^2, 808 nm laser. (b) Different concentrations under a 2 W/cm^2, 660 nm laser. (c) Different power densities of 808 nm laser at the concentration of 42.2 μg/mL. (d) The temperature increment versus the length of PPy-coated Au chains under 3.5 W/cm^2, 808 nm laser irradiation for 5 min at the concentration of 33.8 μg/mL. The initial temperature is 20 °C.

enhanced NIR extinction. The longer NP chains possess a larger size, thus showing the slightly decreased η from Rayleigh scattering.[44] After PPy coating, the composite Au chains with an average length of 1 and 2 NPs exhibit the η increase, whereas longer chains show the η decrease (Table 1), which is seemingly inconsistent with the direct measurement of temperature increment (Figure 3d). This implies that the photothermal transduction is not solely dependent on the η of given materials, but the capability of absorbing light. The longer Au chains possess a larger size and subsequently stronger NIR extinction, thus leading to a more obvious temperature increment (Figure 3d). Nevertheless, η is a basic parameter to estimate the photothermal transduction behavior of given materials.

Table 1 also implies that the PPy shell of composite Au chains may contribute to η and photothermal transduction, in particular for the shorter chains. To reveal the effect of PPy, the composite Au chains with fixed length, but altered PPy thickness, is studied (Figure 2a and Figure S6, Supporting Information). A clear temperature increment from 29.7 to 34.9 °C is observed with increasing the thickness of the PPy shell from 0 to 14.5 nm. In addition, pure PPy NPs solution possesses a broad absorption over 800 nm and the apparent color of dark green (Figure S7, Supporting Information). These facts mean that PPy is capable of absorbing NIR irradiation. Most recently, Liu, Dai, and Zheng took advantage of the strong NIR absorbance of sub-100 nm PPy NPs for photothermal treatment of tumor cells.[13−15] With a few minutes irradiation with an 808 nm laser, the system temperature increases from room temperature to over 50 °C, which can kill tumor cells. The reported η of PPy at 808 nm is 44.7%,[15] which is lower than that of Au chains (Table 1). In particular, the total amount of PPy in our system is less than that of Au. Thus, PPy shells do not play the key role in the photothermal transduction (Figure S6 and Table S1, Supporting Information).

It should be mentioned that, in comparison with the bare Au chains, a PPy-thickness-dependent extinction red shift of composite Au chains is found, which is simultaneously accompanied with an increase of extinction intensity (Figure 2a). In addition, the total temperature increment is always larger than the sum of the contributions from Au chains and the PPy shell. These imply that, besides the Au chains and PPy shell, the improved photothermal effect may be related to the core–shell structure of composite Au chains. Figure 6 indicates the absorption spectra of the Au NPs mixed with different amounts and sizes of PPy NPs. No spectral shift is observed for such mixtures, firmly proving the contribution of Au–PPy composite structures. It is known that the optical plasmon resonance is associated with the collective oscillation of the conduction electrons confined in the NPs.[1] The electron oscillation generates positive cores and delocalized electrons around the cores. According to the Mie theory,[45] the electron vibration in the NPs is confined in a smaller space as they are coated with a polymer shell, which shortens the extent of electron vibration and results in the red shift of plasmon resonance absorption. Moreover, surface polarization can provide a restoring force that directly influences the extent of electron vibration. PPy is a conductive polymer. When PPy is exposed to external irradiation, the electromagnetic field will make it polarization, thus enhancing the restoring force and shortening the extent of electron vibration. Consequently, the formation of composite structures promotes the red shift of the extinction peak to NIR.

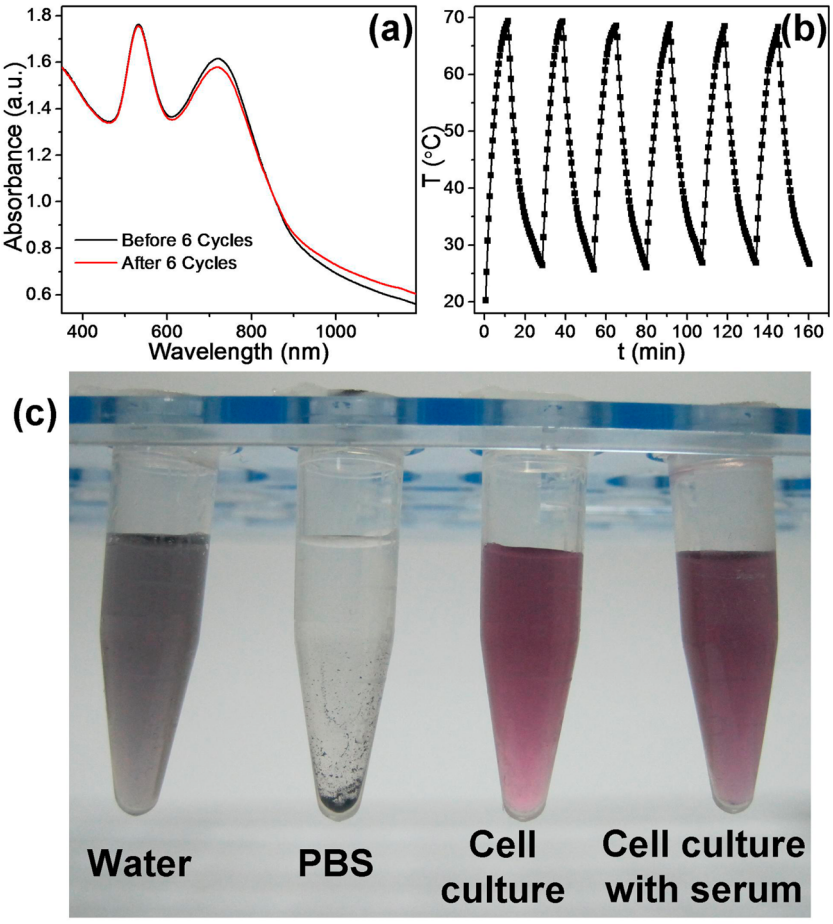

Figure 4. Photothermal (a, b) and physiological (c) stability of PPy-coated chainlike architectures. Absorption spectra before and after irradiation (a), and real-time temperature record (b) of 42.2 μg/mL composite architecture solution that are irradiated by a 3.5 W/cm^2, 808 nm laser from room temperature to top temperature for 6 cycles. (c) The photograph of 21.1 μg/mL composite architectures that are dispersed in water, PBS, and cell culture without and with 10% fetal bovine serum for 7 days.

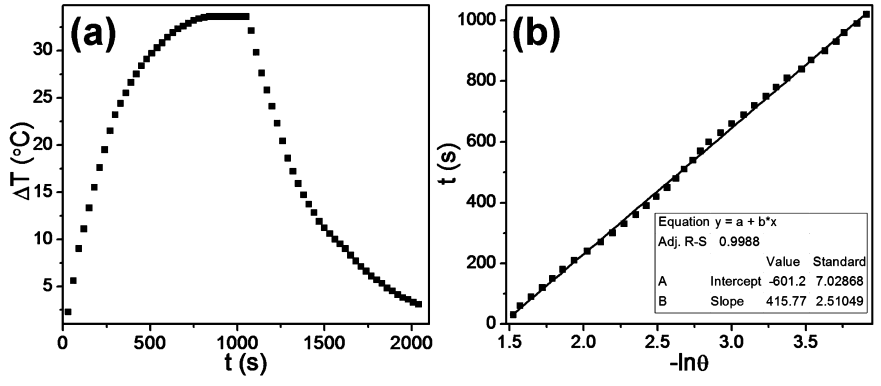

Figure 5. (a) Photothermal effect of the irradiation of the 13.35 μg/mL aqueous solution of PPy-coated Au chains with a 3.5 W/cm^2, 808 nm laser. The solution is irradiated for 1050 s using a 3.5 W/cm^2, 808 nm laser and cooled to room temperature under ambient environment. (b) Time constant for heat transfer from the system is determined to be τ_s = 415.7 s by applying the linear time data from the cooling period (after 1050 s) versus negative natural logarithm of driving force temperature.

The spectral red shift is always accompanied with the increase of extinction intensity. Basically, three parts, namely, Au NP chains, PPy, and the composite structures, contribute to the extinction. Because the amount of Au NPs and PPy are fixed, the extinction intensity increase should result from the composite structures. Extinction intensity is associated with the number of electrons available in the oscillation system.[46] As polarized under external electromagnetic field, the PPy shell can provide additional electrons oscillating with those accounted for the Au surface plasmon resonance. More electrons are supplied by a thicker PPy shell, and hence, the extinction continuously increases with the increase of PPy thickness. Note that, apart from the contribution on electron oscillation, the PPy shell also increases the size of composite Au chains and the subsequent Rayleigh scattering. As a result, the slight decrease of η is observed for the Au chains after PPy coating (Table 1).

dx.doi.org/10.1021/am500715f | ACS Appl. Mater. Interfaces 2014, 6, 5860−5868

Table 1. Summary of the 808 nm Photothermal Transduction Efficiency (η) of Bare and PPy-Coated Au Chains with Different Lengths[a]

		length (NP number)						
		1	2	4	6	8	10	12
η (%)	bare chains	17.8	50.3	71.4	69.2	68.8	68.5	67.2
	composite chains	66.1	70.5	64.4	62.4	62.0	61.4	59.8

[a]For PPy-coated Au chains, the PPy thickness is fixed at 14.5 nm and the concentration of Au NPs is 33.8 μg/mL.

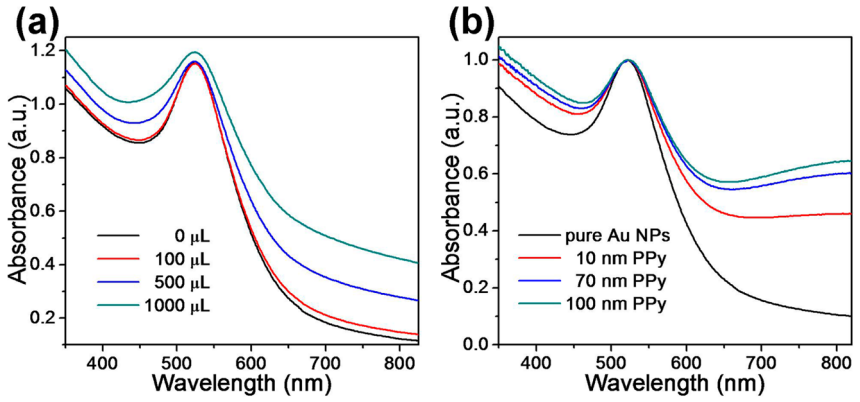

Figure 6. UV−vis absorption spectra of the aqueous Au NPs with the addition of different amounts (a) and sizes (b) of PPy particles. The volume of Au solution is 2 mL. The concentration of PPy is 0.05 mM referring to Py.

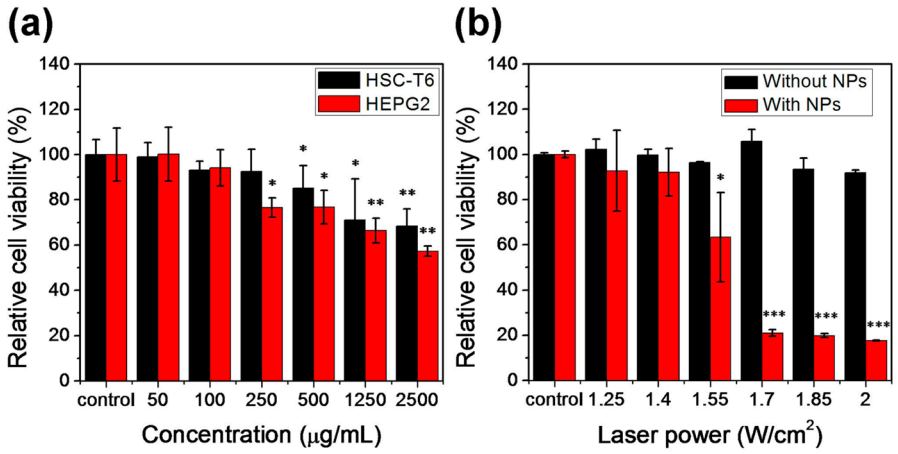

Figure 7. In vitro cell experiments. (a) Cytotoxicity of PPy-coated Au chains, which is tested by incubating HSC-T6 and HEPG2 cells in 100 μL of culture medium with different concentrations of PPy-coated Au chains for 24 h, followed by MTT assay. (b) HEPG2 cell viabilities under 808 nm laser irradiation with different power densities for 3 min in 100 μL of culture medium with and without 0.25 mg/mL PPy-coated Au chains. Data are shown as the means ± standard error of the means; *, $p < 0.05$; **, $p < 0.01$; and ***, $p < 0.001$.

For better revealing the contributions from Au NPs, the PPy shell, and the Au−PPy composite structures, a simple system is compared, namely, single NPs coated with PPy (Figure S8, Supporting Information). For the composite NPs with a 17.4 nm PPy shell, the temperature increment is more than 20 times higher than that of bare NPs (Figure S8f). Extinction spectra clearly exhibit that the composite NPs with thicker PPy possess a higher extinction intensity and red shifted extinction peaks (Figure S8e), consistent with the observation about the composite Au chains. These results also indicate that the contribution of PPy is dominant for PPy-coated single NPs, which is very different from PPy-coated Au NP chains, whereas the contribution from composite structures is similar (Table S1, Supporting Information). The PPy-coated Au chains are further coated with other polymers, such as polystyrene (PS). Additional red shift of the extinction peak is also observed (Figure S9, Supporting Information). Finally, functional groups, such as amine and carboxyl, can be modified on PPy-coated Au architectures via copolymerization route (Figure S10 and Table S2, Supporting Information), thus allowing the further conjugation with biomolecules for photothermal therapy.

One obvious advantage of PPy-coated Au chains over pure PPy NPs is the capability of generating enough heat from smaller nano-objects. For PPy NPs, the photothermal transduction effect relates to their diameter (Figure S7, Supporting Information). Only the PPy NPs with a diameter larger than 70 nm exhibit efficient photothermal transduction.[13] In comparison, PPy-coated single Au NPs already indicate a much stronger photothermal transduction effect, the diameter of which is only 25 nm (Figure 1b). Even for the composite Au chains with a length of 6 NPs, the size is 30 × 70 nm (Figure 1d), still smaller than PPy NPs. It is known that the NP size

dx.doi.org/10.1021/am500715f | ACS Appl. Mater. Interfaces 2014, 6, 5860−5868

greatly affects biodistribution and cellular uptake. Smaller NPs exhibit a decreased footprint, which will shorten uptake and circulation times for in vivo photothermal therapy.

To demonstrate the potentials of PPy-coated Au chains as photothermal agents, the physiological stability in phosphate buffered saline (PBS) and cell culture with and without 10% fetal bovine serum is studied (Figure 4c). After 7 days of incubation, the composite architectures kept stable both in water and in cell cultures. The serious aggregation in PBS is attributed to the reduced electrostatic repulsion at pH 7.4 rather than the deconstruction of the composite architectures. The cytotoxicity is investigated through standard MTT assay of the viabilities of hepatic stellate cells (HSC-T6) and hepatoma cells (HEPG2) (Figure 7a). The HSC-T6 and HEPG2 are incubated in the culture medium for 24 h with the addition of PPy-coated Au chains. As the concentration of PPy-coated Au chains is lower than 100 μg/mL, no obvious toxicity is found for both HSC-T6 and HEPG2. It means that this dosage is safe for both normal cells and tumor cells. Even when the concentration is increased to 500 μg/mL, the relative viabilities remain more than 70%. Such viability is similar with the previously reported photothermal agents of pure PPy particles.[14] The low cytotoxicity is attributed to the biocompatible PPy shell, which suppresses the release of inner toxic composition.[48]

The in vitro photothermal effect is studied by comparing the viabilities of HEPG2 under NIR laser irradiation in the presence and absence of PPy-coated Au chains (Figure 7b). After 4 h of incubation of HEPG2 with 250 μg/mL composite Au chain solution, the cells are irradiated by an 808 nm laser with different power densities for 3 min. After NIR irradiation, the cells are double-stained with fluorescent dyes to count the viabilities.[34] An obvious viability decrease with the increase of power density is found, showing the capability of photothermal tumor cell ablation by PPy-coated Au chains. As the power density reaches 1.7 W/cm^2, the viability already decreases to 20%. In comparison, the 808 nm irradiation in the absence of composite Au chains does not lower the viabilities of HEPG2 in the tested power range. Note that, in the current studies, lower power density and shorter irradiation time are adoptable, because of the higher η of PPy-coated Au chains than the previously reported PPy particles.[14] This exhibits the advantage of PPy-coated Au chains as the competitive photothermal agents of PPy particles by lowering the irradiation power close to the acceptable dosage of the human body, though 1.7 W/cm^2 is still higher than the safety limitation according to the American National Standards Institute Laser Safety Standards (0.33 W/cm^2).

The in vivo photothermal therapy with PPy-coated Au chains is tested using H22 tumor-bearing mice with five mice per group (Figure 8). For the treated group, 0.1 mL of a suspension of 0.5 mg/mL PPy-coated Au chains (the dose is 2 mg/kg) is injected into the tumors. Subsequently, the tumors are irradiated by an 808 nm laser with the power density of 2 W/cm^2. A sharp decrease of tumor volume is observed in comparison to the untreated group, laser-only group, and NP only group (Figure 8a–d). After 14 days of observation, tumors are taken out for photographing and weighing (Figure 8, insets). The average weight of tumors of the treated group is 0.83 g, much lighter than that of the other groups. In addition, the mice of the treated group can live longer than 21 days, whereas all the mice are dead in the other groups after 18 days

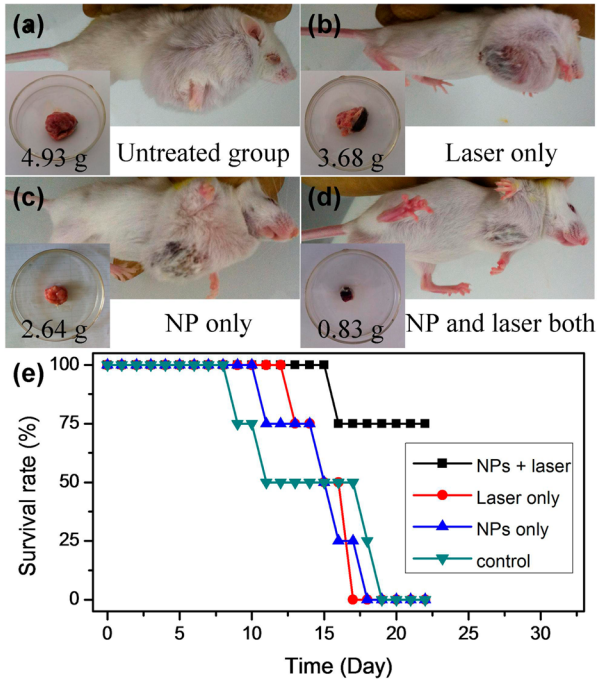

Figure 8. In vivo photothermal therapy. (a–d) Typical photographs for each group. The mice were divided into four groups, namely, untreated group (a), only laser irradiated group (b), only NP injected group (c), and both laser irradiated and NP injected group (d). Insets: typical tumors taken from the aforementioned mice; the average weight is 4.93, 3.68, 2.64, and 0.83 g, respectively. (e) Survival rate of the mice for each group.

(Figure 8e). These results strongly suggest that the PPy-coated Au chains are effective in photothermal treatment of tumors.

CONCLUSIONS

In summary, we demonstrate the good photothermal performance of PPy-coated Au NP chains. The η is up to 70% at 808 nm. The three parts, namely, the chainlike structure of Au NPs, the strong absorption of PPy at the NIR region, and the unique structure of PPy-coated Au NPs, contribute to the photothermal performance. Meanwhile, the PPy shell also enhances the structural stability of the nanocomposites. Because of the good biocompatibility and low toxicity of PPy, the current effort is expected to further promote the practical applications of nanocomposite photothermal agents in establishing novel diagnostic and therapeutic methodologies.

ASSOCIATED CONTENT

Supporting Information

TEM images of bare Au chains, stability of the composite Au chains, device and calculation of photothermal transduction efficiency, effect of PPy thickness on the temperature variation, and characterization of PPy NPs and composite Au chains. This material is available free of charge via the Internet at http://pubs.acs.org.

AUTHOR INFORMATION

Corresponding Authors

*Fax: +86 431 85193423. Tel: +86 431 85159205. E-mail: hao_zhang@jlu.edu.cn (H.Z.).
*E-mail: wanglp@jlu.edu.cn (L.W.).

Notes

The authors declare no competing financial interest.

■ ACKNOWLEDGMENTS

This work was supported by NSFC (21374042, 21174051, 21221063), the 973 Program of China (2014CB643503), the Natural Science Foundation of Jilin Province (201215030, 20140101048JC), and the Special Project from MOST of China.

■ REFERENCES

(1) Jain, P. K.; Huang, X. H.; El-Sayed, I. H.; El-Sayed, M. A. Noble Metals on the Nanoscale: Optical and Photothermal Properties and Some Applications in Imaging, Sensing, Biology, and Medicine. *Acc. Chem. Res.* **2008**, *41*, 1578−1586.

(2) Doane, T. L.; Burda, C. The Unique Role of Nanoparticles in Nanomedicine: Imaging, Drug Delivery and Therapy. *Chem. Soc. Rev.* **2012**, *41*, 2885−2911.

(3) Qin, Z.; Bischof, J. C. Thermophysical and Biological Responses of Gold Nanoparticle Laser Heating. *Chem. Soc. Rev.* **2012**, *41*, 1191−1217.

(4) De, M.; Ghosh, P. S.; Rotello, V. M. Applications of Nanoparticles in Biology. *Adv. Mater.* **2008**, *20*, 4225−4241.

(5) Hirsch, L. R.; Stafford, R. J.; Bankson, J. A.; Sershen, S. R.; Rivera, B.; Price, R. E.; Hazle, J. D.; Halas, N. J.; West, J. L. Nanoshell-Mediated Near-Infrared Thermal Therapy of Tumors under Magnetic Resonance Guidance. *Proc. Natl. Acad. Sci. U.S.A.* **2003**, *100*, 13549−13554.

(6) Von Maltzahn, G.; Park, J.-H.; Agrawal, A.; Bandaru, N. K.; Das, S. K.; Sailor, M. J.; Bhatia, S. N. Computationally Guided Photothermal Tumor Therapy Using Long-Circulating Gold Nanorod Antennas. *Cancer Res.* **2009**, *69*, 3892−3900.

(7) Bardhan, R.; Lal, S.; Joshi, A.; Halas, N. J. Theranostic Nanoshells: From Probe Design to Imaging and Treatment of Cancer. *Acc. Chem. Res.* **2011**, *44*, 936−946.

(8) Kennedy, L. C.; Bickford, L. R.; Lewinski, N. A.; Coughlin, A. J.; Hu, Y.; Day, E. S.; West, J. L.; Drezek, R. A. A New Era for Cancer Treatment: Gold-Nanoparticle-Mediated Thermal Therapies. *Small* **2011**, *7*, 169−183.

(9) Boisselier, E.; Astruc, D. Gold Nanoparticles in Nanomedicine: Preparations, Imaging, Diagnostics, Therapies and Toxicity. *Chem. Soc. Rev.* **2009**, *38*, 1759−1782.

(10) Vogel, A.; Venugopalan, V. Mechanisms of Pulsed Laser Ablation of Biological Tissues. *Chem. Rev.* **2003**, *103*, 577−644.

(11) Melancon, M. P.; Zhou, M.; Li, C. Cancer Theranostics with Near-Infrared Light-Activatable Multimodal Nanoparticles. *Acc. Chem. Res.* **2011**, *44*, 947−956.

(12) Yang, J.; Choi, J.; Bang, D.; Kim, E.; Lim, E.-K.; Park, H.; Suh, J.-S.; Lee, K.; Yoo, K.-H.; Kim, E.-K.; Huh, Y.-M.; Haam, S. Convertible Organic Nanoparticles for Near-Infrared Photothermal Ablation of Cancer Cells. *Angew. Chem., Int. Ed.* **2011**, *50*, 441−444.

(13) Yang, K.; Xu, H.; Cheng, L.; Sun, C.; Wang, J.; Liu, Z. In Vitro and In Vivo Near-Infrared Photothermal Therapy of Cancer Using Polypyrrole Organic Nanoparticles. *Adv. Mater.* **2012**, *24*, 5586−5592.

(14) Zha, Z.; Yue, X.; Ren, Q.; Dai, Z. Uniform Polypyrrole Nanoparticles with High Photothermal Conversion Efficiency for Photothermal Ablation of Cancer Cells. *Adv. Mater.* **2013**, *25*, 777−782.

(15) Chen, M.; Fang, X.; Tang, S.; Zheng, N. Polypyrrole Nanoparticles for High-Performance *in Vivo* Near-Infrared Photothermal Cancer Therapy. *Chem. Commun.* **2012**, *48*, 8934−8936.

(16) Antaris, A. L.; Robinson, J. T.; Yaghi, O. K.; Hong, G.; Diao, S.; Luong, R.; Dai, H. Ultra-Low Doses of Chirality Sorted (6,5) Carbon Nanotubes for Simultaneous Tumor Imaging and Photothermal Therapy. *ACS Nano* **2013**, *7*, 3644−3652.

(17) Kim, J.-W.; Galanzha, E. I.; Shashkov, E. V.; Moon, H.-M.; Zharov, V. P. Golden Carbon Nanotubes as Multimodal Photoacoustic and Photothermal High-Contrast Molecular Agents. *Nat. Nanotechnol.* **2009**, *4*, 688−694.

(18) Li, M.; Yang, X.; Ren, J.; Qu, K.; Qu, X. Using Graphene Oxide High Near-Infrared Absorbance for Photothermal Treatment of Alzheimer's Disease. *Adv. Mater.* **2012**, *24*, 1722−1728.

(19) Gobin, A. M.; Watkins, E. M.; Quevedo, E.; Colvin, V. L.; West, J. L. Near-Infrared-Resonant Gold/Gold Sulfide Nanoparticles as a Photothermal Cancer Therapeutic Agent. *Small* **2010**, *6*, 745−752.

(20) He, J.; Liu, Y.; Babu, T.; Wei, Z.; Nie, Z. Self-Assembly of Inorganic Nanoparticle Vesicles and Tubules Driven by Tethered Linear Block Copolymers. *J. Am. Chem. Soc.* **2012**, *134*, 11342−11345.

(21) Lee, A.; Andrade, G. F. S.; Ahmed, A.; Souza, M. L.; Coombs, N.; Tumarkin, E.; Liu, K.; Gordon, R.; Brolo, A. G.; Kumacheva, E. Probing Dynamic Generation of Hot-Spots in Self-Assembled Chains of Gold Nanorods by Surface-Enhanced Raman Scattering. *J. Am. Chem. Soc.* **2011**, *133*, 7563−7570.

(22) Chen, Z.; Wang, Q.; Wang, H.; Zhang, L.; Song, G.; Song, L.; Hu, J.; Wang, H.; Liu, J.; Zhu, M.; Zhao, D. Ultrathin PEGylated $W_{18}O_{49}$ Nanowires as a New 980 nm-Laser-Driven Photothermal Agent for Efficient Ablation of Cancer Cells In Vivo. *Adv. Mater.* **2013**, *25*, 2095−2100.

(23) Kakiuchida, H.; Takahashi, M.; Tokuda, Y.; Yoko, T. Rewritable Holographic Structures Formed in Organic−Inorganic Hybrid Materials by Photothermal Processing. *Adv. Funct. Mater.* **2009**, *19*, 2569−2576.

(24) Tian, Q.; Tang, M.; Sun, Y.; Zou, R.; Chen, Z.; Zhu, M.; Yang, S.; Wang, J.; Wang, J.; Hu, J. Hydrophilic Flower-Like CuS Superstructures as an Efficient 980 nm Laser-Driven Photothermal Agent for Ablation of Cancer Cells. *Adv. Mater.* **2011**, *23*, 3542−3547.

(25) Hessel, C. M.; Pattani, V. P.; Rasch, M.; Panthani, M. G.; Koo, B.; Tunnell, J. W.; Korgel, B. A. Copper Selenide Nanocrystals for Photothermal Therapy. *Nano Lett.* **2011**, *11*, 2560−2566.

(26) Li, W.; Zamani, R.; Gil, P. R.; Pelaz, B.; Ibáñez, M.; Cadavid, D.; Shavel, A.; Alvarez-Puebla, R. A.; Parak, W. J.; Arbiol, J.; Cabot, A. CuTe Nanocrystals: Shape and Size Control, Plasmonic Properties, and Use as SERS Probes and Photothermal Agents. *J. Am. Chem. Soc.* **2013**, *135*, 7098−7101.

(27) Sau, T. K.; Rogach, A. L. Nonspherical Noble Metal Nanoparticles: Colloid-Chemical Synthesis and Morphology Control. *Adv. Mater.* **2010**, *22*, 1781−1804.

(28) Zeng, J.; Goldfeld, D.; Xia, Y. A Plasmon-Assisted Optofluidic (PAOF) System for Measuring the Photothermal Conversion Efficiencies of Gold Nanostructures and Controlling an Electrical Switch. *Angew. Chem., Int. Ed.* **2013**, *52*, 4169−4173.

(29) Jones, M. R.; Osberg, K. D.; Macfarlane, R. J.; Langille, M. R.; Mirkin, C. A. Templated Techniques for the Synthesis and Assembly of Plasmonic Nanostructures. *Chem. Rev.* **2011**, *111*, 3736−3827.

(30) Lohse, S. E.; Murphy, C. J. The Quest for Shape Control: A History of Gold Nanorod Synthesis. *Chem. Mater.* **2013**, *25*, 1250−1261.

(31) Chen, H.; Shao, L.; Li, Q.; Wang, J. Gold Nanorods and Their Plasmonic Properties. *Chem. Soc. Rev.* **2013**, *42*, 2679−2724.

(32) Lal, S.; Clare, S. E.; Halas, N. J. Nanoshell-Enabled Photothermal Cancer Therapy: Impending Clinical Impact. *Acc. Chem. Res.* **2008**, *41*, 1842−1851.

(33) Yuan, H.; Fales, A. M.; Vo-Dinh, T. TAT Peptide-Functionalized Gold Nanostars: Enhanced Intracellular Delivery and Efficient NIR Photothermal Therapy Using Ultralow Irradiance. *J. Am. Chem. Soc.* **2012**, *134*, 11358−11361.

(34) Li, J.; Han, J.; Xu, T.; Guo, C.; Bu, X.; Zhang, H.; Wang, L.; Sun, H.; Yang, B. Coating Urchin-like Gold Nanoparticles with Polypyrrole Thin Shell to Produce the Photothermal Agents with High Stability and Photothermal Transduction Efficiency. *Langmuir* **2013**, *29*, 7102−7110.

(35) Gao, L.; Fei, J.; Zhao, J.; Li, H.; Cui, Y.; Li, J. Hypocrellin-Loaded Gold Nanocages with High Two-Photon Efficiency for Photothermal/Photodynamic Cancer Therapy in Vitro. *ACS Nano* **2012**, *6*, 8030−8040.

(36) Huang, X.; Tang, S.; Liu, B.; Ren, B.; Zheng, N. Enhancing the Photothermal Stability of Plasmonic Metal Nanoplates by a Core-Shell Architecture. *Adv. Mater.* **2011**, *23*, 3420−3425.
(37) Yavuz, M. S.; Cheng, Y.; Chen, J.; Cobley, C. M.; Zhang, Q.; Rycenga, M.; Xie, J.; Kim, C.; Song, K. H.; Schwartz, A. G.; Wang, L. V.; Xia, Y. Gold Nanocages Covered by Smart Polymers for Controlled Release with Near-Infrared Light. *Nat. Mater.* **2009**, *8*, 935−939.
(38) Tang, Z.; Zhang, Z.; Wang, Y.; Glotzer, S. C.; Kotov, N. A. Self-Assembly of CdTe Nanocrystals into Free-Floating Sheets. *Science* **2006**, *314*, 274−278.
(39) Wang, H.; Chen, L.; Shen, X.; Zhu, L.; He, J.; Chen, H. Unconventional Chain-Growth Mode in the Assembly of Colloidal Gold Nanoparticles. *Angew. Chem., Int. Ed.* **2012**, *51*, 8021−8025.
(40) Zhang, C.-L.; Lv, K.-P.; Cong, H.-P.; Yu, S.-H. Controlled Assemblies of Gold Nanorods in PVA Nanofiber Matrix as Flexible Free-Standing SERS Substrates by Electrospinning. *Small* **2012**, *8*, 648−653.
(41) Liu, K.; Nie, Z.; Zhao, N.; Li, W.; Rubinstein, M.; Kumacheva, E. Step-Growth Polymerization of Inorganic Nanoparticles. *Science* **2010**, *329*, 197−200.
(42) Zhang, H.; Wang, D. Controlling the Growth of Charged-Nanoparticle Chains through Interparticle Electrostatic Repulsion. *Angew. Chem., Int. Ed.* **2008**, *47*, 3984−3987.
(43) Roper, D. K.; Ahn, W.; Hoepfner, M. Microscale Heat Transfer Transduced by Surface Plasmon Resonant Gold Nanoparticles. *J. Phys. Chem. C* **2007**, *111*, 3636−3641.
(44) Johnson, I.; Mer, V. K. L. The Determination of the Particle Size of Monodispersed Systems by the Scattering of Light. *J. Am. Chem. Soc.* **1947**, *69*, 1184−1192.
(45) Prodan, E.; Radloff, C.; Halas, N. J.; Nordlander, P. A Hybridization Model for the Plasmon Response of Complex Nanostructures. *Science* **2003**, *302*, 419−422.
(46) Evanoff, D. D.; Chumanov, G. Size-Controlled Synthesis of Nanoparticles. 2. Measurement of Extinction, Scattering, and Absorption Cross Sections. *J. Phys. Chem. B* **2004**, *108*, 13957−13962.
(47) Turkevich, J.; Stevenson, P. C.; Hillier, J. A Study of the Nucleation and Growth Processes in the Synthesis of Colloidal Gold. *Discuss. Faraday Soc.* **1951**, *11*, 55−75.
(48) Wang, C.; Xu, H.; Liang, C.; Liu, Y. M.; Li, Z. W.; Yang, G. B.; Cheng, L.; Li, Y. G.; Liu, Z. Iron Oxide@Polypyrrole Nanoparticles as a Multifunctional Drug Carrier for Remotely Controlled Cancer Therapy with Synergistic Antitumor Effect. *ACS Nano* **2013**, *7*, 6782−6795.
(49) Yuan, H.; Khoury, C. G.; Wilson, C. M.; Grant, G. A.; Bennett, A. J.; Vo-Dinh, T. In Vivo Particle Tracking and Photothermal Ablation Using Plasmon-Resonant Gold Nanostars. *Nanomedicine* **2012**, *8*, 1355−1366.
(50) Chirico, G.; Pallavicini, P.; Collini, M. Gold Nanostars for Superficial Diseases: A Promising Tool for Localized Hyperthermia? *Nanomedicine* **2014**, *9*, 1−3.
(51) Pallavicini, P.; Donà, A.; Casu, A.; Chirico, G.; Collini, M.; Dacarro, G.; Falqui, A.; Milanese, C.; Sironi, L.; Taglietti, A. Triton X-100 for Three-Plasmon Gold Nanostars with Two Photothermally Active NIR (Near IR) and SWIR (Short-Wavelength IR) Channels. *Chem. Commun.* **2013**, *49*, 6265−6267.
(52) Freddi, S.; Sironi, L.; D'Antuono, R.; Morone, D.; Donà, A.; Cabrini, E.; D'Alfonso, L.; Collini, M.; Pallavicini, P.; Baldi, G.; Maggioni, D.; Chirico, G. A Molecular Thermometer for Nanoparticles for Optical Hyperthermia. *Nano Lett.* **2013**, *13*, 2004−2010.